Chapter 4

Structure of the Metastable Symmetric Ripple Phase

4.1 Introduction

As discussed in chapter-I, metastable ripples are sometimes formed while cooling lipids like DMPC or DPPC from the L_α phase [1]. While the basic structural features of the stable asymmetric ripple has now been well established, even the shape of the metastable ripples is still a topic of debate. In this chapter we discuss the electron density map of the symmetric ripples that we have calculated from our x-ray data. We first discuss the earlier work on this phase. In section-4.2 we describe the freeze fracture experiments and in section-4.3 we describe the x-ray experiments on this phase. In section-4.4 we describe our results and present the electron density maps of this phase. Finally in section-4.5 we summarize our results and speculate about the possible origin of the increased water layer thickness seen in this phase.

The type of ripples that we now know to be metastable and symmetric, were first seen in freeze-fracture experiments [2, 3, 4], where they show up as undulations with wavelength of about 270 Å, typically about 1.8 times the wavelength of the coexisting symmetric ripples. Because of the long wavelength, they are sometimes called Λ-ripples and the shorter wavelength asymmetric ripples are called Λ/2 ripples. From careful analysis of the defect structures present in freeze-fractured samples, the Λ-ripples were shown to have a symmetric shape with a plane of reflection normal

to the ripple wave-vector [5]. Later, x-ray experiments also detected ripples with wavelength about 1.8 times that of the stable asymmetric ripple. The angle γ was found to be $\frac{\pi}{2}$ and layer spacing was found to be about 80 Å which is higher than the layer spacing of about 70 Å seen in the stable symmetric ripples (the values are for DPPC [1]).

4.2 Freeze fracture electron microscopy of metastable ripples

Sackmann, Ruppel and Gebhardt [6] have developed a method to reconstruct the height profiles of ripples from freeze fracture electron micrographs. The sample is prepared by depositing a layer of platinum at an angle of about 45^o (followed by a stabilizing layer of carbon deposited at 90^o) onto a freshly freeze-fractured surface. The method is based on the analysis of the platinum layer thickness which can be determined by electron beam absorption. This thickness is a direct function of the orientation of the local tangent to the membrane surface and thus contains information about the surface profile.

Using this technique, experiments were done on vesicles of DMPC. The Λ ripples were found to have grooves along the maxima (figure-4.1). Thus according to this picture, a Λ ripple has a mirror plane perpendicular to the ripple direction: passing through the groove. No such groove was found in the case of the $\Lambda/2$ ripples. An analysis of the lengths of the arms and the amplitudes of the ripples and of the grooves show that the grooves could be a result of a structure where every second saw-tooth of an asymmetric ripple structure is rotated by 180^o. In this case, two minor arms lie next to each other and form the groove. Thus the ripple is in the form of a series of 'M's.

Zasadzinski and Schneider [7] also analyzed freeze fractured samples of DMPC in the $P_{\beta'}$ phase and arrived at the same conclusion regarding the symmetry of the two kinds of ripples. From the height analysis of Λ ripples of wavelength 220 Å, they

conclude that the amplitude of the Λ ripples is at least 90 Å, the depth of the groove is 20 Å and the total width of the groove is 40 Å.

Because the method of three dimensional reconstruction is not very accurate, the existence of the groove is not well established. Defect analysis of freeze fractured samples on the other hand, is a much more direct method of getting information about the symmetry of the ripples, though it does not yield unambiguous results about the details of the shape (for example, the existence of the groove). Such an analysis was done by Ruppel and Sackmann [5], again on DMPC samples. In the model discussed above, Λ ripples have a two-fold rotation axis. Translations by multiples of a wavelength are allowed along the rippling direction and continuous translations are allowed in a direction perpendicular to both the ripple direction and the mean layer normal. It can be shown that in such a system (plane group: *pm*), stable point defects are allowed whereas line defects are not stable [8]. The point defects (disclinations) are analogous to two-dimensional defects in nematic liquid crystals (see [9] and figure-4.2). As in any system with a two fold axis, half-defects are stable. An analysis of the freeze-fractured surface shows that in the regions where the Λ ripples are present, the defect structure can be reduced to sums of half disclinations. This shows that the Λ ripples have a two fold rotation axis as described before.

In a system where no two-fold rotation axis is present, like in the case of the Λ/2 ripples, only integer strength defects are allowed. These defects are analogous to strength +1 and -1 defects in the c-director field of Smectic-C liquid crystals (see [9] and figure-4.2). An analysis of the Λ/2 ripple domains shows that this is indeed the case though the strength one defects decompose into two half strength defects bound by a finite line-defect. This may happen because the elastic distortions associated with the line-defects, which have a rather wide core is smaller than that associated with a point-defect with a smaller core. Thus the defect analysis of Λ/2 ripples shows that they do not have a two fold rotation axis in the plane that contains

Figure 4.1: The ripple profile for the symmetric ripple as predicted from freeze fracture experiments. The 'M's are the major arms and the 'm's are the minor arms. The grooves are marked 'G'.

the ripple direction and the layer normal (plane group $p1$ or $p2$). This result is in agreement with x-ray diffraction [10, 11] and recent freeze fracture [12] experiments.

4.3 X-ray studies of metastable ripples

The Λ ripples (referred to as the secondary ripple in x-ray literature) are sometimes observed in x-ray experiments. Typically they are much fainter than the $\Lambda/2$ (primary) ripples [1, 13]. The x-ray data from multi-domain samples is difficult to analyze because of the coexistence of the two kinds of ripples. Yao et. al. [1] indexed their diffraction pattern from samples of DPPC cooled from the L_α phase in terms of two lattices; one corresponding to the Λ ripples with wavelength (λ_r) of 266 Å, bilayer separation (d) of 82 Å and $\gamma = 90^o$; the other corresponding to $\Lambda/2$ ripples with λ_r = 136.4 Å, d=70.9 Å and $\gamma = 95^o$. This indexing is consistent with the freeze fracture results.

Rappolt and Rapp [14] argued that the coexistence seen in freeze fracture should not bias the indexing of reflections in x-ray experiments and went on to show that their data (DPPC) can be indexed on a single lattice with λ_r=262 Å, d=86.3 Å and γ=107^0. They phase the reflections by a pattern recognition method and get a structure which is very different from the structure of the $\Lambda/2$ ripples and is also different from the structure of the Λ ripples inferred from freeze fracture experiments discussed above. The bilayers have both thickness and height modulations in a manner such that the water is present in form of pockets in-between the bilayers. The bilayer thickness varies between 39 Å and 44 Å; therefore the chains are thought to be

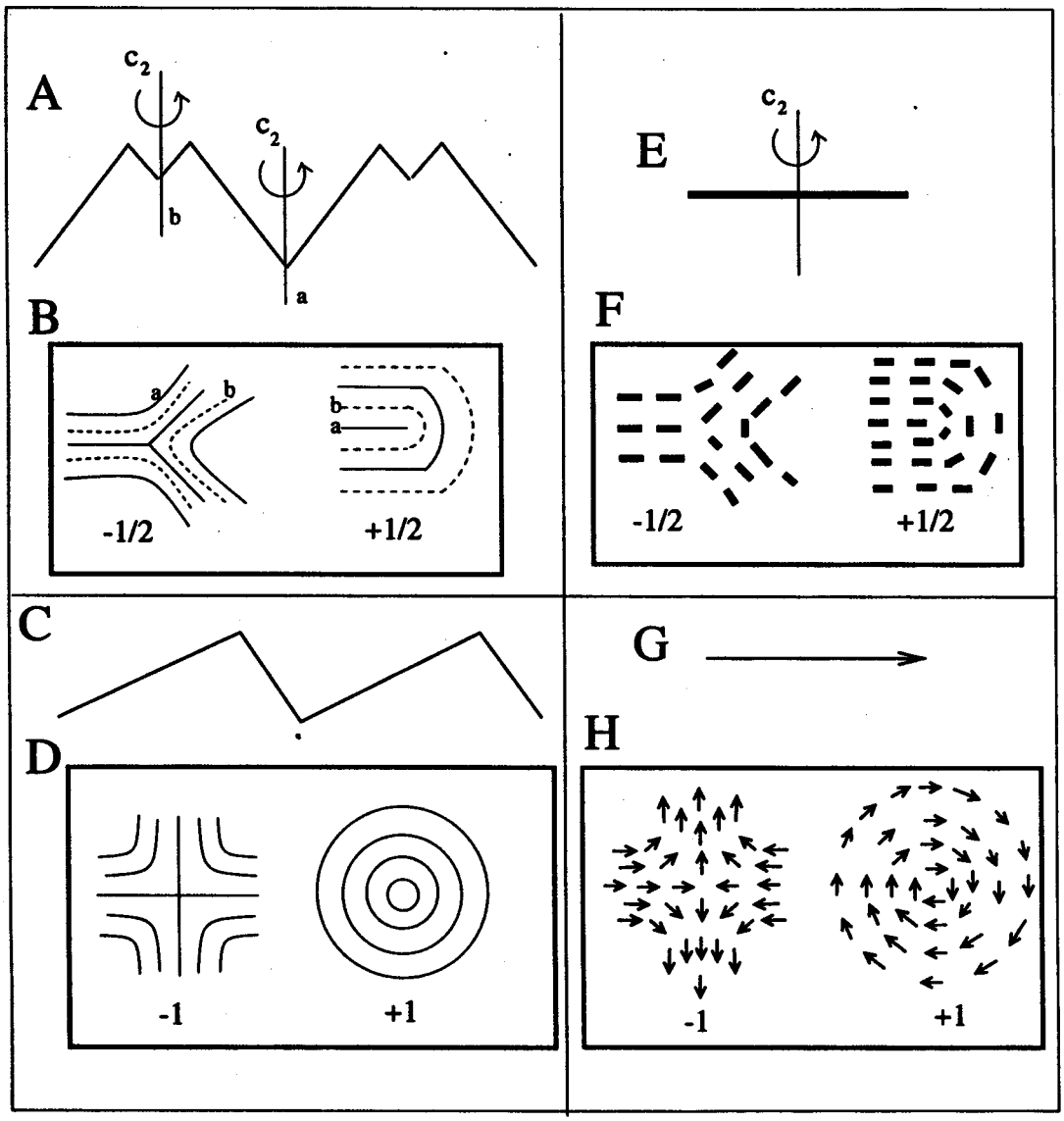

Figure 4.2: Schematic diagram of strength 1/2 and strength 1 defects in two dimensional systems. A: the profile for Λ ripples with two 2-fold (C_2) rotation axis a and b. The symmetry is same as that of an apolar vector or a nematic director. B: half strength defects seen in freeze fracture of the Λ ripples. The solid lines correspond to a and the dashed lines to b. C: profile for $\Lambda/2$ ripples - there is no 2-fold rotation axis and therefore the symmetry is that of a vector. D: strength one defects expected in freeze fracture of $\Lambda/2$ ripples. E: Nematic director, which has the same symmetry as Λ ripples. F: director configuration in half strength defects in nematics. G: a vector, which has the same symmetry as the $\lambda/2$ ripples. An example is the c-vector in Sm_c liquid crystals. H: the c-vector configuration in strength one defects.

all-*trans* and tilted, with the tilt angle varying from 30° to 40°.

Mason et. al. [15] also index their x-ray data from the metastable phase on a single lattice: λ_r=330 Å, d=73 Åand γ=126 Å. They further show that the data of Yao et. al. [1] can also be fitted using this single lattice model, with λ_r=350 Å, d=71 Å and γ=129°. The major problem with this sort of indexing is that it would imply that an altogether different sort of phase with a wavelength of $\approx$ 250 Å is observed in freeze fracture.

4.4 Electron density map of metastable ripples in DPPC

We have calculated electron density maps of the metastable ripples for oriented samples of DPPC. The experiments were performed at the CHESS synchrotron facility (Cornell high-energy synchrotron source, Ithaca, USA) using incident radiation of wavelength 1.3808 Å. The data was collected using a CCD camera. The sample was prepared using the method described in chapter II. The humidity was maintained at 100%. The Λ ripples are formed while cooling the sample from the L_α phase. From the diffraction patterns it can be seen that the angle γ is always $\pi/2$ for the Λ ripples. Thus the indexing in references [14] and [15] are clearly incorrect. In all such pictures, there is coexistence of the Λ phase (with γ=$\pi/2$) and the $\Lambda/2$ phase (with $\gamma \neq \pi/2$). A typical diffraction pattern is shown in figure-4.3. This data corresponds a temperature of 39.2 °C and shows λ_r=254.5 Å, d=79.5 Å and γ=90°. These results are in good agreement with freeze fracture results [5, 7] and with the results of Yao et. al. [1].

The data reduction procedure for calculating the electron density maps is described in chapter-II. Since γ=90° implies an overlap of reflections with Miller indices +k and -k, an assumption that the +k and the -k reflections have the same intensity is necessary. Therefore, the intensity recorded for each satellite reflection has been

Figure 4.3: **A typical diffraction pattern for the metastable ripples at 39.2 °C and 100 % RH.** A small part of the main beam that has escaped the beam stop is seen near the top. Some of the main reflections are over exposed in this picture - this is necessary to get the satellite reflections. The over exposure is corrected for by comparing with an image where exposure time is less. The (1,0) and (2,0) reflections from the asymmetric ripple (seen as weaker spots immediately below the corresponding main reflection from the symmetric ripple) is also present. The angle γ is clearly 90^o.

equally distributed between the +k and -k reflections. The geometrical corrections are applied as before. The corrected intensities are fitted using the modeling and least squares fitting procedure described in chapter-II. To phase the reflections, different initial models for the ripple profile $C(x,z)$ have been tried, but none of them give a completely satisfactory electron density map. The different possible forms for the ripple profile $C(x,z)$ shall be discussed below. For the trans-bilayer profile $T_\psi(x,z)$, model-I where the head-groups and the methyl end group are modeled as delta functions (see chapter-II) was used.

4.4.1 Sawtooth shape (0-groove model)

The simplest choice for $C(x,z)$ is the saw-tooth shaped model that was used to phase the asymmetric ripples (see chapter-II). In the limit where the length of the longer arm is equal to half the wavelength ($\lambda_1 = \lambda_r/2$), the saw-tooth goes to a symmetric triangular shape. The electron density map for the saw-tooth model is given in figure-4.4 and the corresponding observed and calculated structure factors are given

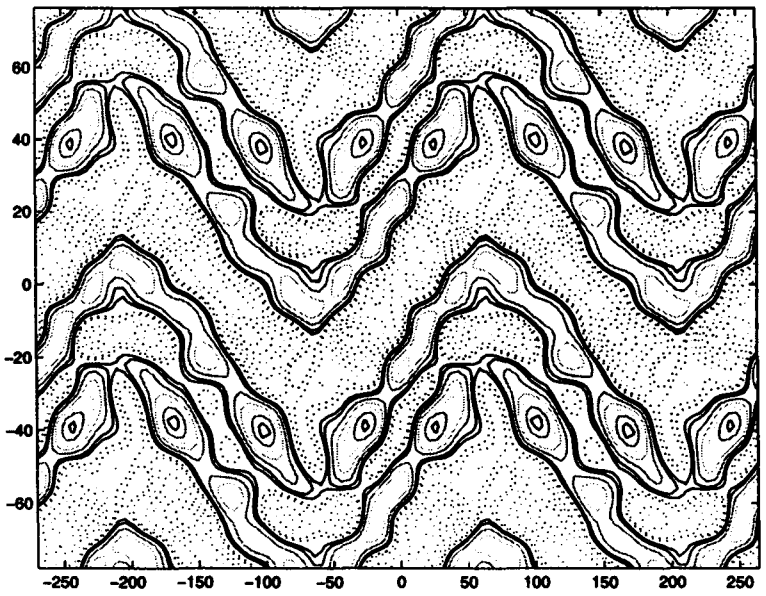

Figure 4.4: **Electron Density Map of the ripple phase of DPPC at temperature = 39.2°C and RH=100% using the 0-groove model.** The positive (negative) contours are represented by solid (dotted) lines. The regions with positive electron density correspond to the head-groups. Note that the thickness of the bilayers is about 50 Å, whereas that of the water region is about 30 Å.

in table-4.1. The phases are determined by the least squares fitting method described in chapter-II but since convergence is poor, the maps are also checked for their goodness using some criteria expected to be satisfied by the electron density distribution. These criteria are: the bilayers are continuous and distinct, bilayers do not cross or touch and the head-group region has a fairly uniform thickness. Maps corresponding to a lower least square deviation are sometimes rejected if the above criterion are not fulfilled. The converged values of the fitted parameters are given in table-4.4.

As can be seen from the figure, the ripple shape has a plane of reflection normal to the ripple wave-vector. The peak-to-peak amplitude of the ripples is about 60 Å, the bilayer thickness varies from about 50 Å to 53 Å and the water layer thickness is about 30 Å. The thickness of the head-group region in one of the monolayers of the bilayer is very small near the peaks; this probably indicates that the initial model chosen differs considerably in the peak region from the real structure.

Table 4.1: **Observed and calculated structure factors for DPPC at temperature = 39.2°C and RH=100% (0-groove model).**

h	k	$\|F_o\|$	$\|F_c\|$	h	k	$\|F_o\|$	$\|F_c\|$
1	0	100.0	-28.3	2	-5	46.2	-32.7
1	1	78.1	91.9	3	0	43.6	12.9
1	-1	78.1	-88.3	3	1	5.2	-2.8
1	2	67.4	-78.6	3	-1	5.2	3.8
1	-2	67.4	-80.3	3	2	36.7	-15.7
1	3	96.7	25.5	3	-2	36.7	-14.7
1	-3	96.7	-32.6	3	3	8.9	2.4
1	4	47.5	8.1	3	-3	8.9	-6.9
1	-4	47.5	4.4	3	4	10.3	36.6
2	0	114.8	34.7	3	-4	10.3	28.4
2	1	5.2	-29.9	3	5	28.7	-54.3
2	-1	5.2	31.7	3	-5	28.7	53.3
2	2	68.1	-58.8	3	6	44.1	31.3
2	-2	68.1	-46.3	3	-6	44.1	41.0
2	3	90.4	125.0	3	7	48.1	0.6
2	-3	90.4	-112.6	3	-7	48.1	8.9
2	4	107.7	-94.7	4	0	29.4	9.4
2	-4	107.7	-99.1	5	0	56.4	-16.9
2	5	46.2	17.6	6	0	24.8	-2.0

4.4.2 Triangular ripple with groove at both extrema (2-groove model)

From the electron density map obtained with the saw-tooth model, it is clear that this shape is only an approximation to the real shape especially near the peaks. Therefore, keeping in mind the freeze fracture result of Sackmann et. al. [6], the initial ripple profile was taken to be a triangular shape with grooves (with variable depths) at the peaks and troughs. Though the freeze fracture shows grooves only at the peaks and not at the troughs, a model with grooves at both the extrema was used since the one-groove model is non-centrosymmetric and therefore difficult to phase. It was expected that some features of the structure may be obtained even with the centrosymmetric model, which could be used as input for the non-centrosymmetric model discussed later.

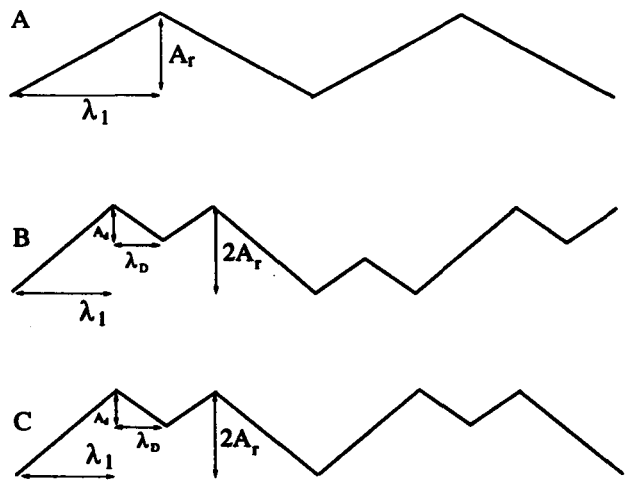

Figure 4.5: Schematic diagram of the model ripple profile for the (A) 0-groove, (B) 2-groove and (C) 1-groove models.

$C(x,z)$ in this case is:

$$C(x,z) = \delta(z - u(x))$$

$u(x)$ is given by $u(x) = m(x+c)$, where

$m = \frac{A_r}{\lambda_1}$	$c = 2(\lambda_1 + \lambda_D)$	*when*	$-2(\lambda_1 + \lambda_D) < x < -(\lambda_1 + 2\lambda_D)$
$m = -\frac{A_d}{\lambda_D}$	$c = (\lambda_1 + 2\lambda_D - A_r\frac{\lambda_D}{A_d})$	*when*	$-(\lambda_1 + 2\lambda_D) < x < -(\lambda_1 + \lambda_D)$
$m = \frac{A_d}{\lambda_D}$	$c = \lambda_1 + A_r\frac{\lambda_D}{A_d}$	*when*	$-(\lambda_1 + \lambda_D) < x < -\lambda_1$
$m = \frac{-A_r}{\lambda_1}$	$c = 0$	*when*	$-\lambda_1 < x < \lambda_1$
$m = \frac{Ad}{\lambda_D}$	$c = -(\lambda_1 + A_d\frac{\lambda_D}{A_d})$	*when*	$\lambda_1 < x < \lambda_1 + \lambda_D$
$m = \frac{-A_d}{\lambda_D}$	$c = -(\lambda_1 + 2\lambda_D - A_r\frac{\lambda_D}{A_d})$	*when*	$\lambda_1 + \lambda_D < x < \lambda_1 + 2\lambda_D$
$m = \frac{A_r}{\lambda_1}$	$c = -2(\lambda_1 + \lambda_D)$	*when*	$\lambda_1 + 2\lambda_D < x < 2(\lambda_1 + \lambda_D)$

Here A_r is the ripple amplitude, A_d is the groove depth, λ_D is half the width of the groove and λ_1 is $(\lambda_r/4 - \lambda_D)$, λ_r is the wavelength of the ripple (see figure 4.5). This model gives the best fit for A_d=0. This is a special case where the top and the bottom of the triangular shape is flat. The electron density maps calculated with this model is shown in figure-4.6. The corresponding observed and calculated structure factors are given in table-4.2. The converged values of the fitted parameters are given in table-4.4.

The ripple shape clearly has two 2-fold rotation axis in the plane containing the rippling direction and the layer normal (plane of the paper). In figure-4.6 the thickness of the bilayer varies from about 32 Å for the region near the peak to about 56 Å for

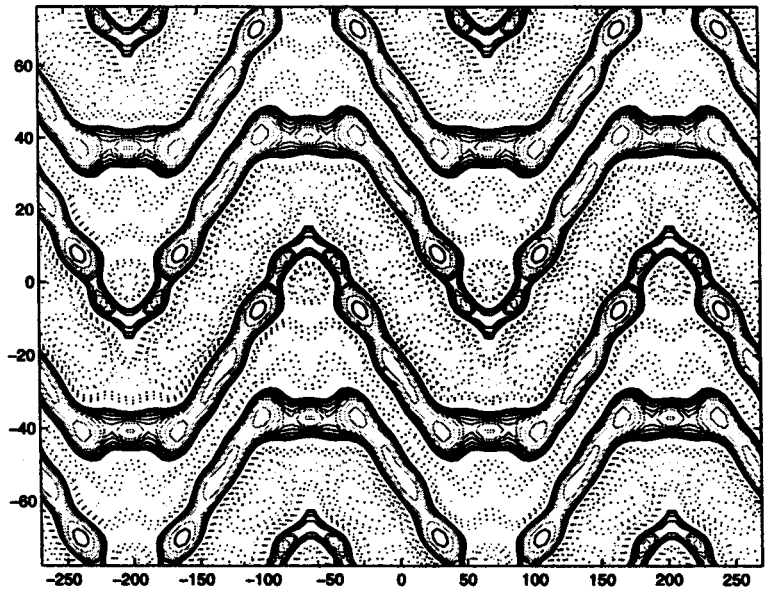

Figure 4.6: **Electron Density Map of the ripple phase of DPPC at 39.2°C and 100% RH for the 2-groove model.** The positive (negative) contours are represented by solid (dotted) lines. The regions with positive electron density correspond to the head-groups. Note that the thickness of the bilayers is about 50 Å, whereas that of the water region is about 30 Å.

Table 4.2: **Observed and calculated structure factors for DPPC at 39.2°C and 100% RH. (2-groove model)**

h	k	$\|F_o\|$	$\|F_c\|$	h	k	$\|F_o\|$	$\|F_c\|$
1	0	100.0	-34.3	2	-5	46.2	16.5
1	1	78.1	-107.5	3	0	43.6	11.1
1	-1	78.1	94.8	3	1	5.2	-2.8
1	2	67.4	-71.1	3	-1	5.2	9.7
1	-2	67.4	-72.0	3	2	36.7	-19.8
1	3	96.7	-31.2	3	-2	36.7	-21.6
1	-3	96.7	19.2	3	3	8.9	7.9
1	4	47.5	8.0	3	-3	8.9	-1.5
1	-4	47.5	10.1	3	4	10.3	38.6
2	0	114.8	60.4	3	-4	10.3	37.1
2	1	5.2	11.9	3	5	28.7	53.2
2	-1	5.2	-28.9	3	-5	28.7	-49.3
2	2	68.1	-68.7	3	6	44.1	32.7
2	-2	68.1	-65.4	3	-6	44.1	30.6
2	3	90.4	-129.1	3	7	48.1	5.7
2	-3	90.4	110.3	3	-7	48.1	-1.2
2	4	107.7	-82.2	4	0	29.4	8.6
2	-4	107.7	-75.6	5	0	56.4	4.0
2	5	46.2	-31.2	6	0	24.8	1.8

rest of the bilayer. This indicates that most of the chains are fully stretched and have zero mean tilt. The water layer thickness is about 30 Å and the peak to peak amplitude of the ripple is about 50 Å.

Both the centrosymmetric shapes considered so far yield electron density maps where the top and bottom monolayers of the bilayers seem to have different shapes. In case of the 2-groove model, wherever the top monolayer is flat, the bottom monolayer has a sharp maximum and vice versa. This sort of shape where the two monolayers of the bilayer have different profiles, is highly unlikely. Therefore we conclude that though the gross features like the amplitude, layer thickness etc. can be reliably read off these electron density maps, the map is not good enough to detect the finer features. Since centrosymmetric structures fail to give a good electron density map of the feature at the top, the structure is probably non-centrosymmetric.

4.4.3 Non-centrosymmetric profile (1-groove model)

The ripple profile suggested by freeze fracture experiments [6, 7] indicates the presence of a groove only at one of the extrema of the triangular shape. This shape, with one groove per wavelength, is non-centrosymmetric and hence the phase factor is no longer constrained to be ± 1. Since now Φ can be any angle, it is no longer possible to follow a multidimensional fitting procedure to obtain the phases because the model does not always converge to any reasonable point.

$C(x, z)$ in this case is:

$$C(x, z) = \delta(z - u(x))$$

where $u(x)$ is given by $u(x) = m(x + c)$,

$$\begin{array}{llll}
m = \frac{A_r}{\lambda_1} & c = 2(\lambda_1 + \lambda_D) & when & -2(\lambda_1 + \lambda_D) < x < -(\lambda_1 + 2\lambda_D) \\
m = -\frac{A_d}{\lambda_D} & c = (\lambda_1 + 2\lambda_D - A_r \frac{\lambda_D}{A_d}) & when & -(\lambda_1 + 2\lambda_D) < x < -(\lambda_1 + \lambda_D) \\
m = \frac{A_d}{\lambda_D} & c = \lambda_1 + A_r \frac{\lambda_D}{A_d} & when & -(\lambda_1 + \lambda_D) < x < -\lambda_1 \\
m = \frac{-A_r}{\lambda_1} & c = 0 & when & -\lambda_1 < x < \lambda_1 + \lambda_D \\
m = \frac{A_r}{\lambda_1} & c = -2(\lambda_1 + \lambda_D) & when & \lambda_1 + \lambda_D < x < 2\lambda_1
\end{array}$$

Here A_r is the ripple amplitude, A_d is the groove depth, λ_D is half the width of the

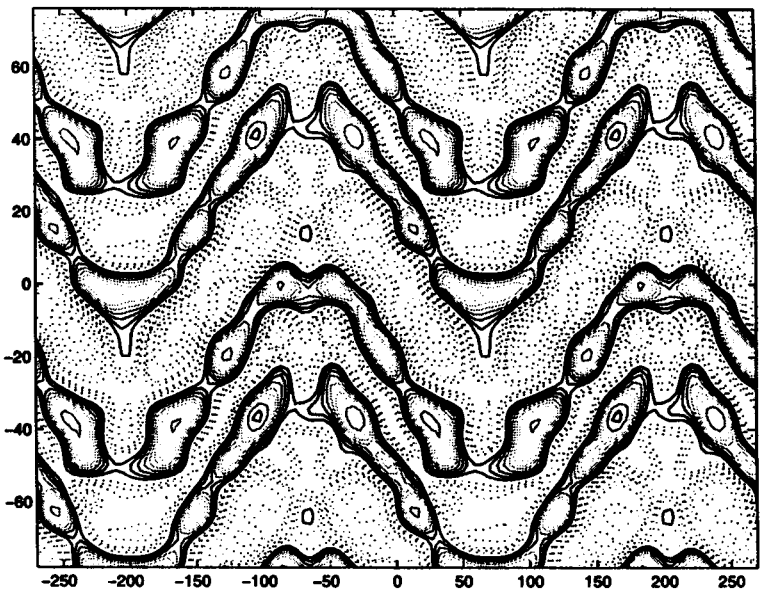

Figure 4.7: Electron Density Map of the ripple phase of DPPC at 39.2°C and 100% RH using the 1-groove model. The positive (negative) contours are represented by solid (dotted) lines. The regions with positive electron density correspond to the head-groups. Note that the thickness of the bilayers is about 50 Å, whereas that of the water region is about 30 Å.

groove and λ_1 is $(\lambda_r/4 - \lambda_D)$, λ_r is the wavelength of the ripple (see figure-4.5). All the ripple parameters like A_r, the bilayer thickness L, the angle ψ and the ratio of head-group to terminal methyl group electron density R_{hm} are fixed at the values measured from the electron density maps obtained with the centro-symmetric models. The depth of the groove is allowed to vary and a one dimensional least squares fit is performed. This is followed by iterative least square fits of each of the variables taken one at a time till the variations from one fit to the next are negligible. The maps are checked for continuity and other criterion for goodness as discussed earlier. The values of A_r and A_d reported in freeze fracture experiments [7] have also been tried as inputs but the electron density maps corresponding to values close to these are found to be unphysical. The best electron density map that could be obtained is given in figure-4.7 and the corresponding calculated structure factors and phases are given in table-4.3. The converged values of the fitted parameters are given in table-4.4.

The overall shape of the final structure is similar to the structure obtained using the

Table 4.3: **Observed and calculated structure factors and phases Φ_c for DPPC at 39.2°C and 100% RH: $-\pi < \Phi_c < \pi$ (1-groove model)**

h	k	$\|F_o\|$	$\|F_c\|$	Φ_c	h	k	$\|F_o\|$	$\|F_c\|$	Φ_c
1	0	100.0	34.5	3.0	2	-5	46.2	18.0	0.4
1	1	78.1	107.7	3.1	3	0	43.6	11.6	-0.3
1	-1	78.1	94.9	0.0	3	1	5.2	3.6	-2.5
1	2	67.4	71.1	3.1	3	-1	5.2	10.0	-0.2
1	-2	67.4	72.1	3.1	3	2	36.7	21.7	2.7
1	3	96.7	31.2	3.1	3	-2	36.7	22.8	2.8
1	-3	96.7	19.5	0.2	3	3	8.9	8.6	-0.4
1	4	47.5	10.2	-0.7	3	-3	8.9	1.7	-2.8
1	-4	47.5	10.1	0.0	3	4	10.3	38.7	-0.1
2	0	114.8	61.3	-0.2	3	-4	10.3	37.5	-0.1
2	1	5.2	12.9	-0.4	3	5	28.7	53.2	-0.1
2	-1	5.2	31.4	2.7	3	-5	28.7	49.3	3.1
2	2	68.1	68.7	3.1	3	6	44.1	33.8	0.2
2	-2	68.1	65.6	3.1	3	-6	44.1	31.0	0.2
2	3	90.4	130.0	3.0	3	7	48.1	6.7	-0.6
2	-3	90.4	110.7	-0.1	3	-7	48.1	2.0	2.2
2	4	107.7	83.3	3.0	4	0	29.4	10.5	-0.6
2	-4	107.7	75.9	3.1	5	0	56.4	8.2	-1.0
2	5	46.2	31.3	3.1	6	0	24.8	2.2	0.5

centrosymmetric models. The peak-to-peak amplitude is about 48 Å and the layer thickness varies from about 46 Å to about 55 Å. The finer features are again poorly resolved. A shallow depression is seen at the peak but no corresponding elevation is evident at the trough. This non-centrosymmetric structure is to be expected, given the constraints on the starting model. Even with this non-centrosymmetric model, the electron density map is not good enough to make any meaningful comment on the details of the structure of the ripples near the peaks.

The final converged values of the various parameters, the crystallographic R factor and the least square deviation (Σ) are given in table-4.4. The converged values of the parameters are important only because they are used to calculate the structure factors and hence the phases of the reflections. The phases of the reflections are not very sensitive to small changes in these parameters and these parameters are not used directly to calculate the electron density maps. Therefore, the values of these

Table 4.4: The converged values of the parameters using the three models:

	0-groove	2-groove	1-groove
λ_1	131.5	57.4	124.6
A_r	67.0	18.0	30.0
A_d		0.0	17.0
ψ	0.0	0.0	0.0
R_H/R_M	1.2	1.5	1.2
L	49.0	49.0	49.0
R	0.5	0.5	0.5
Σ	309034	252169	46510

measured from the electron density maps are different from the converged values given in table-4.4.

4.4.4 Patterson Map

A plot of the fourier transform of the intensities (rather than the structure factors) is called the Patterson map. The Patterson map represents the convolution of the electron density function with its centrosymmetric image. Patterson map peaks occur at positions that correspond to interatomic vectors within the real space unit cell. Therefore, if there are N atoms in an unit cell, there are $N(N-1)$ peaks in the Patterson map. The use of Patterson map to determine a complicated structure like the present case is limited but a comparison of the Patterson maps obtained using the observed intensities and the intensities calculated from each of the above models may give some clue about the relative accuracy of each of the three models.

The Patterson map calculated with the observed structure factors is given in figure-4.8. The central peak corresponds to the self correlation of the atoms and is the dominant feature. There are a few relatively weaker peaks and a weak "X"-pattern is seen centered on the central maximum. We are unable to understand these features of the map though a comparison with the Patterson maps obtained using the calculated structure factors show that the 0-groove and the 1-groove models capture some of these features.

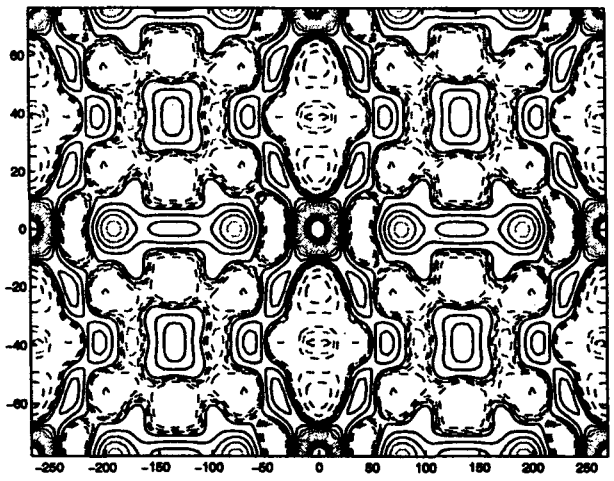

Figure 4.8: **Patterson map of data set given in table I.** The positive (negative) contours are represented by solid (dashed) lines.

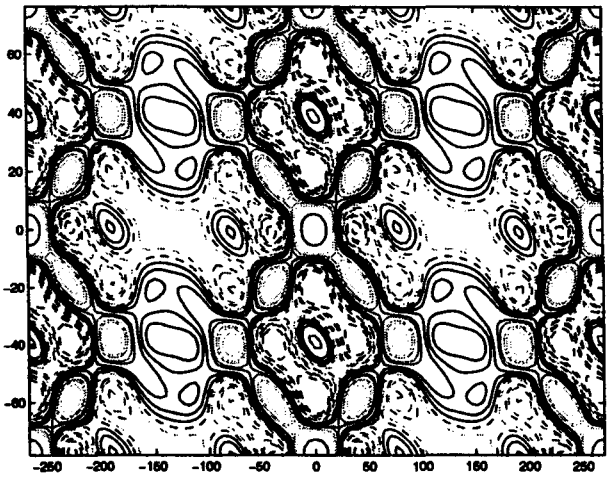

Figure 4.9: Patterson map using intensities calculated from the 0-groove model. The positive (negative) contours are represented by solid (dashed) lines.

For comparison, the Patterson map from the asymmetric ripple phase (data of Wack and Webb [16]) is shown in figure-4.12. The central peak is the dominant feature here- it consists a thick tilted "X" with unequal arms. This represents the correlation within each arm of the saw-tooth.

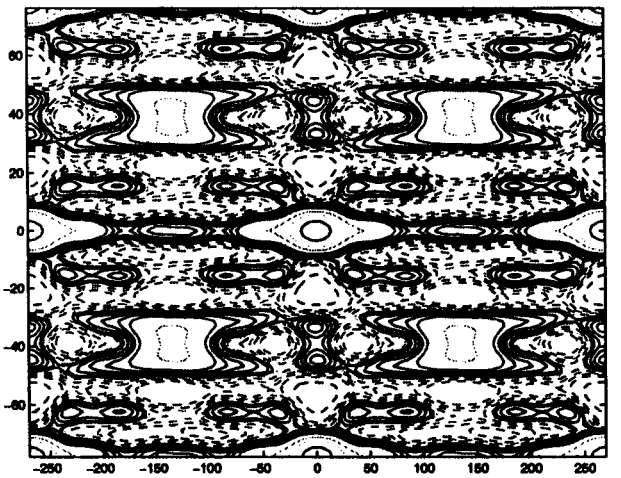

Figure 4.10: **Patterson map using intensities calculated from the 2-groove model.**The positive (negative) contours are represented by solid (dashed) lines.

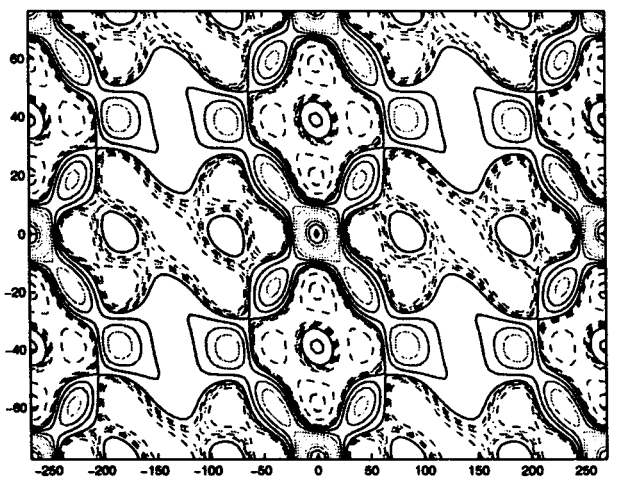

Figure 4.11: **Patterson map using intensities calculated from the 1-groove model.**The positive (negative) contours are represented by solid (dashed) lines.

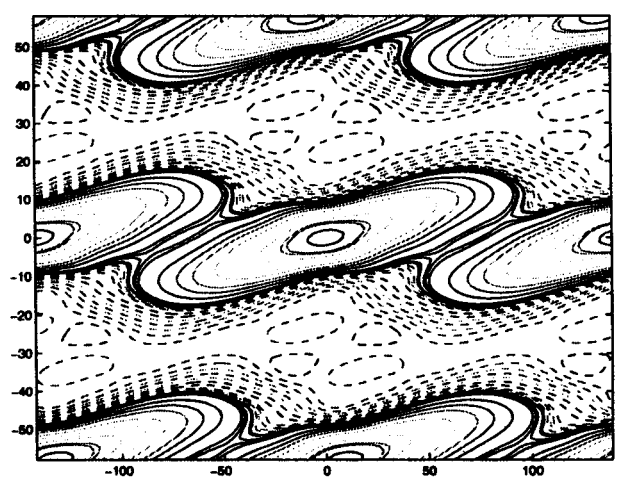

Figure 4.12: **Patterson map using observed intensities for the asymmetric ripple (data from [16].**The positive (negative) contours are represented by solid (dashed) lines.

4.5 Conclusion

From the electron density maps presented here, it is clear that the metastable ripples have a two fold rotation axis in the plane containing the layer normal and the ripple wave-vector. The amplitude is about 50 Å and is in agreement with freeze fracture results of an amplitude of atleast 45 Å. The thickness of the water layer is about 30 Å, about 10 Å more than in the asymmetric ripples. A layer thickness of about 50 Å indicates that the chains are mostly all-*trans* at least away from the peaks. The shape of the ripples near the peaks is poorly resolved. Though our calculations indicate that the structure is non-centrosymmetric with probably a groove at the peak, depth of this groove is likely to be much less than the values estimated from freeze fracture experiments [5, 6, 7].

The interesting question here is what determines the thickness of the water layers and why this thickness should be greater in the symmetric ripples than in the asymmetric ripples. The long range interactions possible in these systems are the electrostatic interaction and the Helfric interaction [17] arising from thermal fluctuation of the bilayers. Since the chains are mostly all-*trans* and rigid, the Helfric interaction should be negligible. The only possible source of coulomb interactions is through the dipolar head groups. Since the configuration of the head-groups in the two kinds of ripples are not known, the details of dipolar interactions can not be further commented upon. An indirect way of checking this hypothesis would be to look at lipid-water systems with added salt so that the electrostatic interaction is screened. Another interesting possibility is to introduce divalent cation that are known to increase the layer spacing [18] and check if the ripples go from asymmetric to symmetric when they swell.

Bibliography

[1] H. Yao, S. Matuoka, B. Tenchov, and I. Hatta, Biophys. J. **59**, 252 (1991).

[2] P. Pinta da Silva, J. Microsc. **12**, 185 (1971).

[3] A. J. Verkleij, P. H. J. Ververgaert, L. L. M. Van Deenen and P. F. Elbers, Biochim. Biophys. Acta **288**, 326 (1972).

[4] P. H. J. Ververgaert, A. J. Verkleij, P. F. Elbers and L. L. M. Van Deenen , Biochim. Biophys. Acta **311**, 320 (1973).

[5] D. Ruppel and E. Sackmann, J. Phys. (Paris). **44**, 1025 (1983).

[6] E. Sackmann, D. Ruppel and C. Gebhardt, Liquid Crystals of One - and Two-Dimensional Order, W. Helfrich and G. Heppke (ed.), Springer Series in Chemical Physics 11, Springer-Verlag, 1980.

[7] J. A. N. Zasadzinski and M. B. Schneider, J. Phys. (Paris) **48**, 2001 (1987).

[8] N. D. Mermin, Rev. Mod. Phys. **51**, 591 (1979).

[9] P. G. deGennes and J. Prost, The Physics of Liquid Crystals, Clarendon Press - Oxford, 1993.

[10] A. Tardieu, V. Luzzati, and F. C. Reman, J. Mol. Biol. **75**, 711 (1973).

[11] W.-J. Sun, S. Tristram-Nagle, R. M. Suter, and J. F. Nagle, Proc. Natl. Acad. Sci. USA **93**, 7008 (1996).

[12] J. T. Woodward and J. A. Zasadzinski, Phys. Rev. E **53**, R3044 (1996). J. T. Woodward and J. A. Zasadzinski, Biophys. J. **72**, 964 (1997).

[13] S. Matuoka, H. Yao, S. Kato and I. Hatta, Biophys. J. **64**, 1456 (1993)

[14] M. Rappolt and G. Rapp, Eur. Biophys. J., **24**, 381 (1996).

[15] P. C. Mason, B. D. Gaulin, R. M. Epand, G. D. Wignall and J. S. Lin, Phys. Rev. E, **59**, 3361 (1999).

[16] D. C. Wack and W. W. Webb, Phys. Rev. A **40**, 2712 (1989).

[17] W. Helfrich, Z. Naturforsch. **33a**, 305 (1978).

[18] L. J. Lis, W. T. Lis, V. A. Parsegian and R. P. Rand, Biochem. **20**, 1771 (1981). A. Watts, K. Harlos, W. Maschke and D. Marsh, Biochim. Biophys. Acta **510** 63 (1978).